Two-dimensional Infrared Spectroscopy of vibrational polaritons of molecules in an optical cavity.

Prasoon Saurabh$^{a1,\,a)}$ and Shaul Mukamel$^{a1,\,b)}$

^{a}*Department of Chemistry, University of California, Irvine,*

CA 92697

(Dated: 8 October 2018)

Strong coupling of molecular vibrations to an infrared cavity mode affects their nature by creating dressed polariton states. We show how the single and double vibrational polariton manifolds may be controlled by varying the cavity coupling strength, and probed by a time domain 2DIR technique, Double Quantum Coherence (DQC). Applications are made to the amide-I (CO) and amide-II (CN) bond vibrations of $N-methylacetamide$ (NMA).

PACS numbers: 42.79.Gn, 78.47.jh,78.47.N-,82.53.Kp

$^{a)}$Electronic mail: psaurabh@uci.edu

$^{b)}$Electronic mail: smukamel@uci.edu

I. INTRODUCTION

Elementary physical and chemical properties of molecules can be modified by coupling them to the optical modes of a cavity thus forming strongly coupled $matter + field$ states known as polaritons[1,2]. These have been widely studied in atoms. Electronic polaritons in molecules have been extensively studied both experimentally and theoretically[3–5]. Vibrational polaritons in the infrared has been recently demonstrated in molecular aggregates[6–9] and in semiconductor nano-structures[10–12]. The radiation matter coupling is related to cavity frequency ω_c by, $g_i = \sqrt{N}\boldsymbol{\mu}_i \cdot \boldsymbol{e}_c\sqrt{(\hbar\omega_c/2\epsilon_0 V)}$, where, N is the number of molecules. $\boldsymbol{\mu}_i$ is the transition dipole moment of the mode i, $\boldsymbol{e}_c$ is the cavity electric field vector, ϵ_0 is vacuum permittivity, and V is the cavity mode volume[1,6–9,13,14]. While strong coupling to cavity modes has been realized even for a single atom, $N = 1$,[1,2,15] polaritons in organic molecules were reported for large $N(\sim 10^{17})$[6]. With the advent of anomalous refractive index materials[16,17], sub-wavelength Fabry-Perot microcavities[18], and nanocavities[19] it may become possible to achieve strong cavity coupling of single molecules.

Coherent multidimensional infrared spectroscopy is a powerful time domain tool that can probe anharmonicities and vibrational energy relaxation pathways[20–24]. Vibrational polaritons were experimentally reported[6,8,9] and calculated[7,25] recently. Multidimensional spectroscopic studies for electronically excited states in semiconductor cavity for nano-particles like $In_{0.04}Ga_{0.96}As$ has been demonstrated[12,27]. Similarly, electronic exciton-polariton interactions of quantum wells in microcavity[28] has also been reported. Bipolaritons generated using four wave mixing techniques have been used as efficient entangled photon source[29,30].

In this article, we calculate 2DIR signals for vibrational polaritons, focusing specially on the double quantum coherence (DQC) technique. Studying DQC of molecular vibrational polaritons in optical cavity can be used to study the effects of strong couplings on the vibrational anharmonicities and consequently allow us to control these anharmonicities. We introduce DQC signal in next section (Sec.II), we then study single vibrational mode (Amide-I of NMA) coupled to a single mode cavity and calculate DQC in section (Sec.III), followed by two vibrational modes (Amide-I+II of NMA) coupled to a single mode cavity (Sec.IV); and finally conclude in Sec. V.

II. VIBRATIONAL POLARITONS AND THEIR DQC SIGNAL

Vibrational modes (Fig. 1) coupled to an infrared cavity under the Rotating Wave Approximation (RWA) are described by the hamiltonian[6–9,31–33],

$$H_0 = \omega_c(\theta)a^\dagger a + \sum_i^m \omega_i b_i^\dagger b_i + \sum_{i \neq j}^m J_{ij} b_i^\dagger b_j$$
$$- \sum_{ij}^m \frac{\Delta_{ij}}{2} b_i^\dagger b_j^\dagger b_i b_j + \sum_{i,j=1}^m g_i \left(a^\dagger b_i + b_i^\dagger a \right), \tag{1}$$

where, $a(a^\dagger)$ and $b(b^\dagger)$ are annihilation(creation) operators for the cavity photon, and vibrational excitation respectively, which satisfy boson commutation relations, $[a, a^\dagger] = 1$; $[b_i, b_j^\dagger] = \delta_{ij}$ and $\hbar = 1$. $\omega_c(\theta) = \omega_0 \left(1 - \frac{\sin^2(\theta)}{n_{eff}^2}\right)^{-1/2}$, is the angle-dependent cavity energy with ω_0 being cavity cut-off (or maximum) energy and, θ the angle of incidence to the cavity mirrors. We set $\theta = 0°$ for simplicity. ω_i is vibrational frequency of mode i. J_{ij} is the scalar coupling between two vibrational modes i and j, while Δ_{ij} is the anharmonicity between respective modes. Finally, the coupling strength of vibrational modes i to an optical mode is, g_i as described in introduction.

The cavity volume ($V = (\lambda/n_{eff})^3$) depends on cavity resonance wavelength (λ) and effective intra-cavity refractive index (n_{eff})[1,13,14]. Decreasing n_{eff} can also be used for strong coupling to single molecular vibrational excitation, for instance, when the refractive indices of one of the two layers' of a Distributed Bragg Reflector (DBR) Fabry-Perot is equal to the empty cavity refractive index n_c, say $n_c = (n_2 \veebar n_1)$, then $n_{eff} = \sqrt{n_1 n_2}$. In this case, choosing either one of the layers to be material with anomalous refractive index may decrease $n_{eff} < 1$[18]. The vacuum Rabi splitting Ω_R of mode i is $2\hbar g_i$.

DQC is a four wave mixing signal generated by three chronologically ordered pulses with wavevectors $\boldsymbol{k}_1$, $\boldsymbol{k}_2$ and $\boldsymbol{k}_3$ and detected by with a fourth pulse in the direction, $\boldsymbol{k}_{III} = \boldsymbol{k}_1 + \boldsymbol{k}_2 - \boldsymbol{k}_3$ (Fig.1 (e))[21,26]. The signal is recorded versus three time delays t_1, t_2 and t_3. We assume a three polariton manifold as shown in Fig. 1. Using the ladder diagrams for DQC (Fig. 1e) in polariton basis, which diagonalizes the first three and last terms of Eq. 1 (Fig. 1, Sec.SI of supplementary information[34]), we see that system oscillates with frequency $\Omega_{eg} = \Omega_e - \Omega_g$ during time delay $t_1 = \tau_2 - \tau_1$ and with frequency $\Omega_{fe} = \Omega_f - \Omega_e$ during delay $t_2 = \tau_3 - \tau_2$ in both contributing diagrams (Fig. 1e). After the third pulse the system oscillates either with frequency $\Omega_{e'g}$ or $\Omega_{e'f}$ during the delay $t_3 = \tau_4 - \tau_3$. For harmonic case,
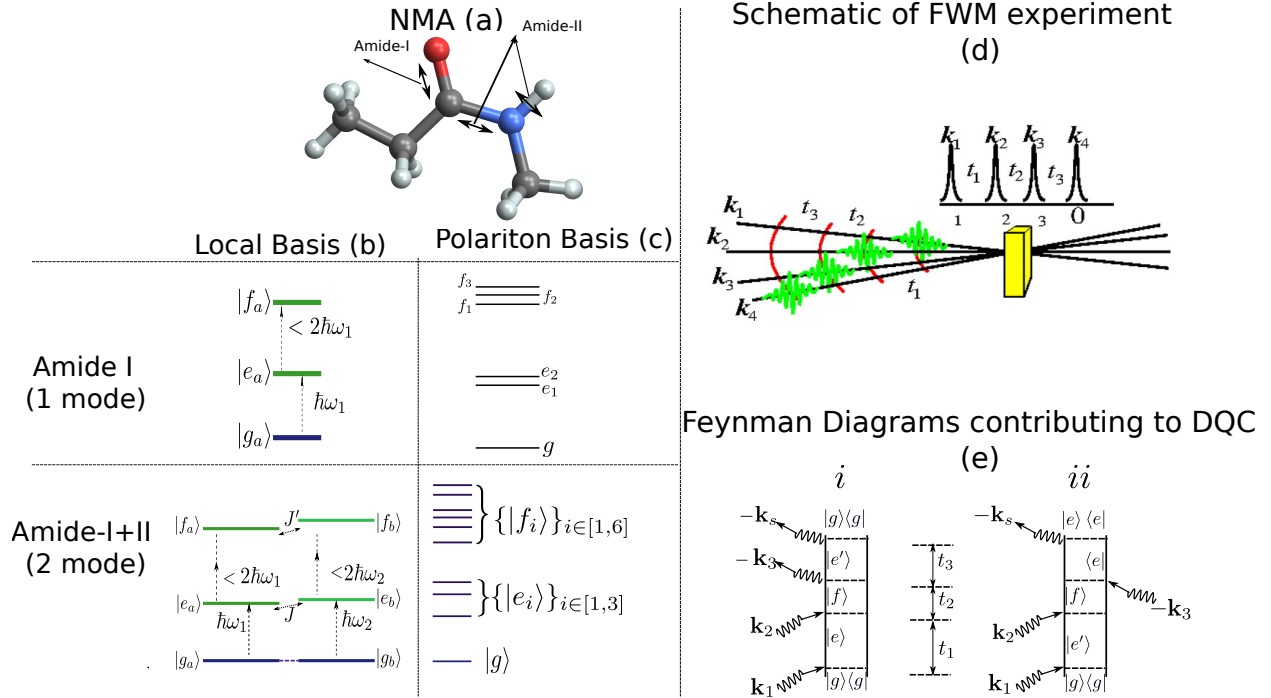
FIG. 1: Amide-I ($C = O$ symmetric stretch) and Amide-II (CN symmetric stretch $+ NH$ bend) vibrations are represented using double sided arrow for $N - Methylacetamide$ in (a). Eigen-energies of Amide-I and coupled Amide-I and Amide-II motifs in local basis and polariton basis (see Sec.SI of supplementary information[34] for detail) are given in (b) and (c) respectively. (d) schemes the FWM experiment, the yellow sample is the DBR Fabry-Perot cavity coupled to molecular vibrations (see text for detail) and, (e) shows the relevant ladder diagrams contributing to double quantum coherence (DQC) technique.

$\Omega_{e'g} = \Omega_{e'f}$ where the DQC signal vanishes. A 3D signal $\mathcal{S}(t_3, t_2, t_1)$, which can be written as double Fouier transform with respect to t_2 and t_3 as[21],

$$\mathcal{S}(\Omega_3, \Omega_2, t_1) = \int \int_0^\infty dt_3 dt_2 e^{i(\Omega_3 t_3 + \Omega_2 t_2)} \mathcal{S}(t_3, t_2, t_1).$$ (2)

Upon expanding in polariton eigenstates, the signal with time delay $t_1 = 0$ becomes,

$$\mathcal{S}(\Omega_3, \Omega_2, t_1 = 0) = \sum_{ee',f} \frac{1}{(\Omega_2 - \Omega_{fg} + i\gamma_{fg})}$$

$$\left[\mu_{e'f}\mu_{ge'}\mu_{fg}\mu_{ge} \frac{1}{\Omega_3 - \Omega_{e'g} + i\gamma_{e'g}} \right.$$

$$\left. - \mu_{ge'}\mu_{e'f}\mu_{fg}\mu_{eg} \frac{1}{\Omega_3 - \Omega_{fe} + i\gamma_{fe}} \right].$$ (3)

Where, μ_{ij} is the polariton transition dipole from states in manifold $j \to i$ while γ_{ij} is the respective dephasing. Note that the polariton eigenstates depend on the effective cavity
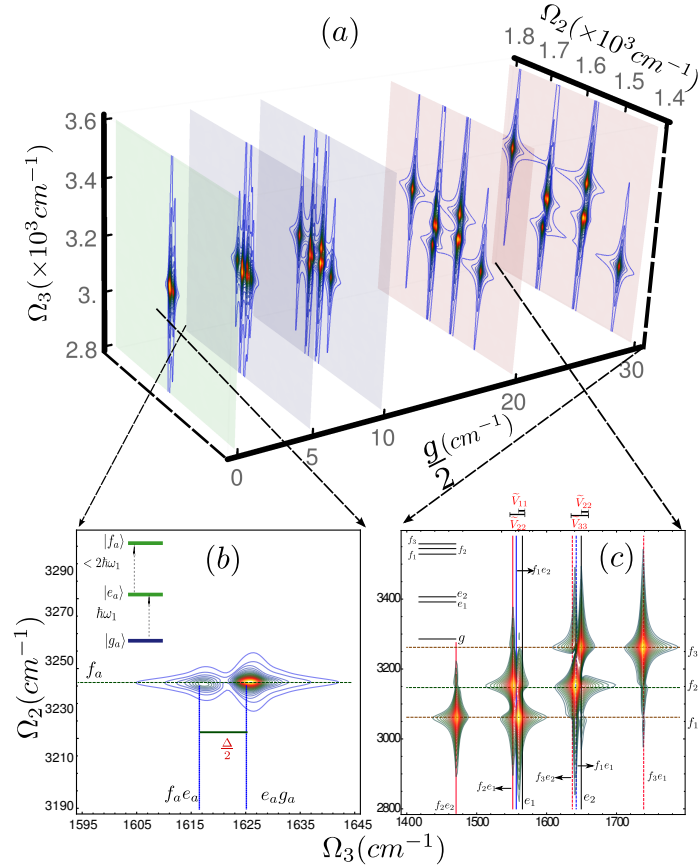
4

FIG. 2: (a) Absolute value of DQC signal (Eq. 3) for Amide-I vibrations of NMA, as we vary coupling strength (g) from no (green plane), weak (blue planes) and strong (red planes) coupling regimes. (b) Schematic representation of DQC signal (zoomed in the grey square at $g = 0 cm^{-1}$) with all possible peaks identified as intersections of different lines. (c) Same result but for strong coupling and the last panel. The lines are: i) Ω_{fe} labelled as $f_i e_j$ (dashed blue lines), ii) Ω_{eg} labelled as e_j (black solid lines), iii) Ω_{fg} labelled as f_i and appropriate anharmonicities (Δ_{ij} in local basis or $\widetilde{V}_{ii}$ in polariton basis) respectively. We wish to spectrally resolve (b) to (c).

coupling strengths, $\widetilde{g}_i \left(= \sqrt{Ng_i^2 - \frac{1}{4}(\kappa - \gamma_i)^2} \right)$, where κ is cavity decay rate, and γ_i is dephasing rate of respective mode[13]. Tuning the cavity coupling allows to control spectral structures of the singly and doubly excited vibrational polariton manifolds (Fig.2 and can be captured using DQC as illustrated in the following section (Sec. III).

5

TABLE I: Parameters used in this work. ω_0 is cavity cut-off frequency. $\omega_{1,2}$ are vibrational exciton (1,2) ($Amide - I$, $Amide - II$) energies[37,38], $\gamma_{1,2}$ are their respective dephasing rates, J_{ij} is harmonic scalar coupling, and Δ_{ij} are exciton-exciton interaction energies.

(in cm^{-1})	Cavity	Amide-I	Amide-I+II
Energy	$\omega_0=1625$	$\omega_1=1625$	$\omega_1=1625$, $\omega_2=1545$
Dephasing	$\kappa=0$	$\gamma_1=20$	$\gamma_1 = \gamma_2=20$
Anharmonicities			$\Delta_{11}=15, \Delta_{22}=11$
(Local basis)	$\Delta_{00} = 0$	$\Delta_{11}=15$	$\Delta_{21} =$
			$\Delta_{12}=10$
Scalar coupling	-	-	$J_{12}=15$
Eff. refractive ind. Anharmonicities	$n_{eff} =0.5$	-	-
(Polariton basis)		$\widetilde{V}_{ij} = \frac{\Delta_{ij}}{2}\lvert X_i\rvert^2\lvert X_j\rvert^2$	

III. A SINGLE VIBRATIONAL MODE COUPLED TO SINGLE CAVITY MODE

The Amide motifs ($O = C - N - H$) link the amino-acid in peptides containing fundamental structural information, for instance, backbone geometry, interactions with hydrogen bonds and dipole-dipole interactions[35]. 2D spectroscopy of the amide-I and II symmetric vibrations (Fig. 1e) have been studied[20,36]. We focus on the Amide-I vibrations in NMA (Table. I). We consider a single Amide-I stretch mode in resonance with the cavity mode and large anharmonicity ($\Delta_{ij} > \gamma_{ij}$) with varying coupling strengths $\widetilde{g}_1$ ranging from 0 to 80 cm^{-1} (Table. I). For a single vibrational mode (Fig.1), the three polariton manifolds have a ground state (g), two single excited states (e) and three doubly excited states (f). Furthermore, for detuning ($\delta = \omega_1 - \omega_c$), the polariton basis modifies the anharmonicity $\Delta_{11}(\rightarrow \widetilde{V}_{11} = 16\Delta_{11}\lvert\widetilde{g}_1^4/(\delta^2 - 16\widetilde{g}_1^2)^2\rvert)$.

Using Eq. 3 and ladder diagrams (Fig. 1e) the signals $\lvert\mathcal{S}_i(\Omega_3, \Omega_2, 0)\rvert$, $\lvert\mathcal{S}_{ii}(\Omega_3, \Omega_2, 0)\rvert$ and $\lvert\mathcal{S}(\Omega_3, \Omega_2, 0) = \lvert\mathcal{S}_i(\Omega_3, \Omega_2, 0) + \mathcal{S}_{ii}(\Omega_3, \Omega_2, 0)\rvert$ are shown in Fig. 3 and 4 in left, center and right columns respectively (sec. III). Absolute values are shown to illustrate peak assignments and affects of varying coupling strengths ($\widetilde{g}_i$). For completness, the respective absorptive

(Im) and dispersive (Re) parts of the DQC signals are shown in Sec.SIIIA in[34]. The peak splittings depends on coupling strengths ($\widetilde{g}_i$) and polariton anharmonicities ($\widetilde{V}_{ij}$) and are given Sec.SV of [34].

Free molecule (Fig. 3): The Amide-I vibrations in NMA (without cavity) is a simple three level system as shown in Fig. 1. Under this condition, $e_1 = e_2$ and $f_1 = f_2 = f_3$, thus we only observe single peak resonant at $\Omega_{fg} = 3168 cm^{-1}$ on Ω_2 axis. The peaks due to $|\mathcal{S}_i(\Omega_3, \Omega_2, 0)|$ (Fig. 3(a)) shows $\Omega_{eg} = 1625 cm^{-1}$ resonance, while $|\mathcal{S}_{ii}(\Omega_3, \Omega_2, 0)|$ (Fig. 3(b)) shows resonance at $\Omega_{fe} = 1617 cm^{-1}$ along Ω_3 axis. The total signal (Fig. 3(c)) thus shows two peaks due to resonances at Ω_{eg} and Ω_{fe}.
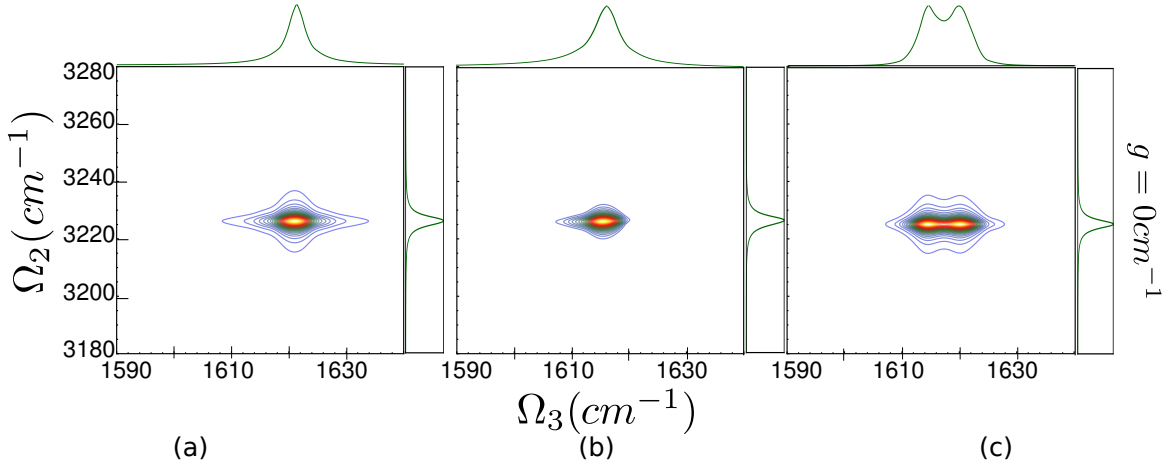

FIG. 3: DQC signals for Amide-I vibrations in NMA using Eq. 3 and ladder diagrams (Fig. 1e): (a) $|\mathcal{S}_i(\Omega_3, \Omega_2, 0)|$ with resonance at $\Omega_{eg} = 1625 cm^{-1}$, (b)$|\mathcal{S}_{ii}(\Omega_3, \Omega_2, 0)|$ with resonance at $\Omega_{fe} = 1617 cm^{-1}$ and (c)$|\mathcal{S}(\Omega_3, \Omega_2, 0)|$ with resonances at $\Omega_{eg} = 1625 cm^{-1}$ and $\Omega_{fe} = 1617 cm^{-1}$. The linear projections along each axis is shown in green. For simplicity, cavity field vector $\boldsymbol{e}_c$ is assumed to be mostly parallel to molecular vibrational transition dipole μ_m. Amide-I vibrations (ω_1) is resonant to cavity cutoff frequency $\omega_0 = 1625 cm^{-1}$. The anharmonicity are assumed $\Delta_{11} = 15 cm^{-1}$ (Table I).

Weak coupling regime (Fig. 4-top row) with $\widetilde{g}=20 cm^{-1}$: Upon varying the coupling strength, there are two singly excited and three doubly excited polariton states (Fig. 1 b-c, Sec SII-S1 of[34]). We thus observe that all $|\mathcal{S}_i(\Omega_3, \Omega_2, 0)|$, $|\mathcal{S}_{ii}(\Omega_3, \Omega_2, 0)|$ and $|\mathcal{S}(\Omega_3, \Omega_2, 0)|$ show three distinct peaks along Ω_2 axis with energies resonant to $\Omega_{f_1 g} = 2\Omega_{e_1 g} - \widetilde{V}_{11}$, $\Omega_{f_2 g} = 2\Omega_{e_1 g}$ and $\Omega_{f_3 g} = 2\Omega_{e_2 g} - \widetilde{V}_{33}$ respectively. Along Ω_3 axis, $|\mathcal{S}_i(\Omega_3, \Omega_2, 0)|$ (Fig. 4(top,left)) shows peak resonance at $\Omega_{e_1 g}$ and $\Omega_{e_2 g}$ with splitting $\sim \widetilde{g}$. The $|\mathcal{S}_{ii}(\Omega_3, \Omega_2, 0)|$ (Fig. 4(top,

middle)) has six distinct peaks at energies resonant to Ω_{f_2,e_2}, Ω_{f_2,e_1}, Ω_{f_1,e_2}, Ω_{f_3,e_2}, Ω_{f_1,e_1}, Ω_{f_3,e_1} in increasing order respectively. The $|\mathcal{S}(\Omega_3,\Omega_2,0)|$ (Fig. 4(top, right)) has diminished peaks at $\Omega_{f_2e_1}$ and $\Omega_{f_3e_2}$ due to destructive interference of $\Omega_{f_2e_1}$ with Ω_{e_1g} and $\Omega_{f_3e_2}$ with Ω_{e_2g} resonances.
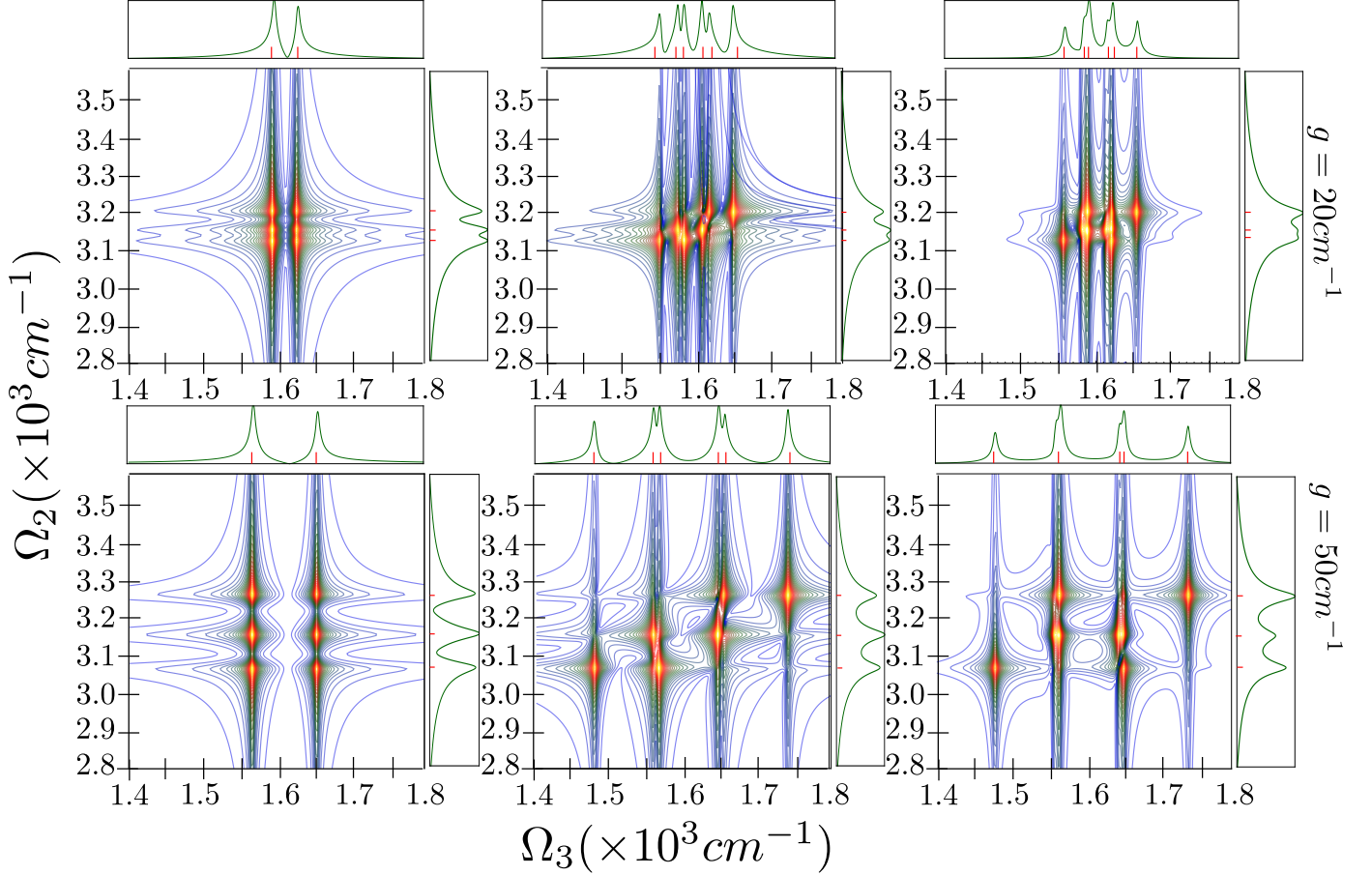

FIG. 4: DQC signals using Eq. 3 and ladder diagrams (Fig. 2b): *Columns* (left$-$)$|\mathcal{S}_i(\Omega_3,\Omega_2,0)|$ with resonance at Ω_{e_1g} and Ω_{e_2g}; (middle$-$)$|\mathcal{S}_{ii}(\Omega_3,\Omega_2,0)|$ with resonance at Ω_{f_2,e_2}, Ω_{f_2,e_1}, Ω_{f_1,e_2}, Ω_{f_3,e_2}, Ω_{f_1,e_1}, Ω_{f_3,e_1} ; and (right$-$)$|\mathcal{S}(\Omega_3,\Omega_2,0)|$ with respective resonances for Amide-I vibrations in NMA with cavity coupling *rows*: $(a)20cm^{-1}$ and $(a)50cm^{-1}$. The linear projections along each axis is shown in green. For simplicity, cavity field vector $\boldsymbol{e}_c$ is assumed to be mostly parallel to molecular vibrational transition dipole μ_m. Amide-I vibrations (ω_1) is resonant to cavity cutoff frequency $\omega_0 = 1625cm^{-1}$. The anharmonicity are assumed $\Delta_{11} = 15cm^{-1}$ (Table I)

Strong coupling regime (Fig. 4-bottom row) with $\widetilde{g} = 50cm^{-1}$: The signals corresponding to $|\mathcal{S}_i(\Omega_3,\Omega_2,0)|$ (Fig. 4(bottom, left)), $|\mathcal{S}_{ii}(\Omega_3,\Omega_2,0)|$ (Fig. 4(bottom, middle)) and

$|\mathcal{S}(\Omega_3, \Omega_2, 0)|$ (Fig. 4(bottom, right)) show peaks corresponding to Ω_{f_1g}, Ω_{f_2g} and Ω_{f_3g} along Ω_2 axis. Projections on Ω_3 axis for $|\mathcal{S}_{ii}(\Omega_3, \Omega_2, 0)|$ six peaks assigned as in weak coupling case, however the peak splitting between resonance pairs with energies $(\Omega_{f_2e_1}, \Omega_{f_1e_2})$ and $(\Omega_{f_3e_2}, \Omega_{f_1e_1})$ remains relatively constant and proportional to respective contributing anharmonicities. The total signal shows six peaks due to $\Omega_{f_2e_1}$ and $\Omega_{f_3e_2}$ diminished because of destructive interferences from resonances of singly excited polaritons.

This partial cancellation of peaks puts an upper bound on strong coupling strengths for fully resolved DQC signals. Furthermore by changing t_1, we can observe the dynamics in singly and doubly excited polariton manifolds to obtain bountiful information regarding lifetimes of molecular vibrational bipolaritons. In case of zero detuning ($\delta = \omega_1 - \omega_c = 0$), the doublet peak splitting due to $\widetilde{V}_{11}$ is independent of coupling strength *i.e.*, $\widetilde{V}_{11} = \Delta/32$. Thus DQC can be used as direct measurements of anharmoncities due to vibrational polariton-polariton interactions for vanishing detuning cases. One has to be careful however, for $\delta \neq 0$ cases; as such conditions allow the anharmonicities to vary non-trivially ($\sim 16\Delta_{11}|\widetilde{g}_1^4/(\delta^2 - 16\widetilde{g}_1^2)^2|$). This may cause destructive interference of different peaks along Ω_3 axis.

IV. POLARITONS FOR TWO VIBRATIONAL MODES AND THEIR DQC SIGNAL

We now couple the Amide-I and Amide-II vibrations (Fig. 1,[36]) of a single NMA molecule ($N = 1$) to an infrared cavity. We next calculate the double quantum coherence (DQC) signals for vibrational molecular polaritons (Fig. 1 (e), Eq. 3) utilizing Eqs.S2-S5 (of supplementary material[34]).

The overlapping of peaks due to anharmonicities is better illustrated in case of Amide-I+II vibrations coupled to single mode cavity. We next present three coupling regimes for such a condition. We assume $\widetilde{g}_1/\widetilde{g}_2 = constant$ for simplicity. The remainder of relevant parameters are shown in Table I.

No cavity (Fig. 6)(a): The coupled Amide-I+II vibrations of NMA is effectively a three level system with two singly excited states and three doubly excited states in absence of cavity coupling. The two singly excited states are resonant with Ω_{e_1g} and $\Omega{e_2g}$. The three doubly excited states are resonant with frequencies $\Omega_{f_1g} = 2\Omega_{e_1g} - \Delta_{11}$, $\Omega_{f_2g} = \Omega_{e_1g} + \Omega_{e_2g}$ and $\Omega_{f_3g} = 2\Omega_{e_2g} - \Delta_{22}$ (Sec. SII of supplementary material [34], Table I). These peaks are observed
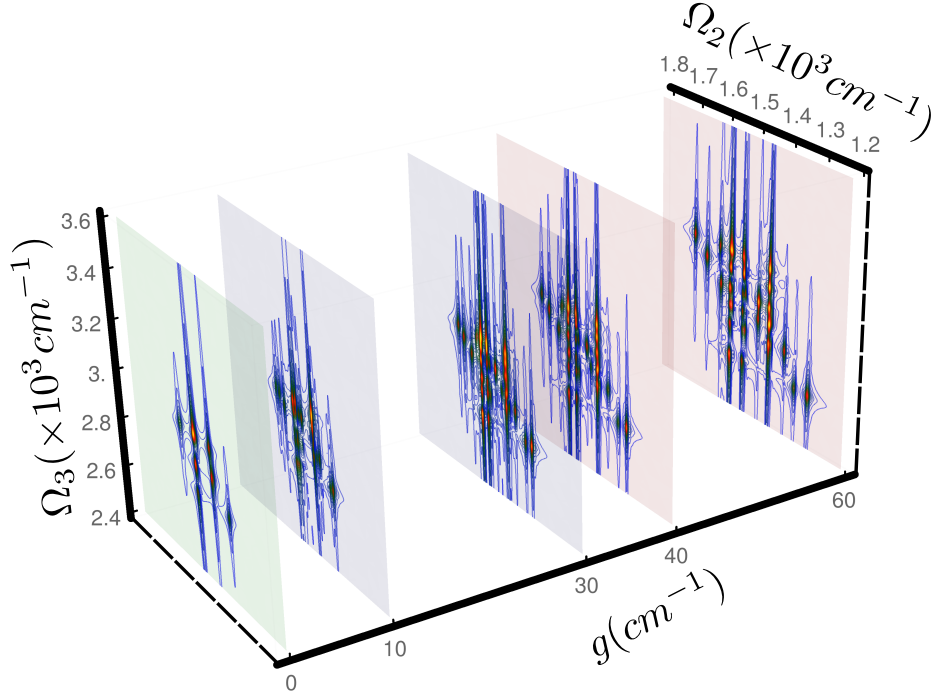
FIG. 5: Modulus of DQC signal for Amide-I+II vibrations in NMA with varying cavity coupling $(0cm^{-1} \to 60cm^{-1})$. Cavity field vector $\boldsymbol{e}_c$ is assumed to be mostly parallel to molecular vibrational transition dipole μ_m. Amide-I vibrations (ω_1) is resonant to cavity cutoff frequency $\omega_0 = 1625cm^{-1}$ and $\omega_2 = 1540cm^{-1}$. The anharmonicies $\Delta_{11} = 15cm^{-1}$ and $\Delta_{22} = 11cm^{-1}$ (Table I).

along Ω_2 axis. Whereas, we only observe four peaks along Ω_3 axis in (Fig. 6(a, right column)) because the tuples $(\Omega_{f_2e_1}, \Omega_{f_1e_2}), \Omega_{e_1g})$ and $(\Omega_{f_3e_2}, \Omega_{f_1e_1}), \Omega_{e_2g})$ cannot be resolved due to anharmonicities $(\Delta_{ii},$ Table I).

Weak coupling regime with $\widetilde{g} = 10cm^{-1}$ (Fig. 6)(b): Under these conditions, we observe five peaks along Ω_2 axis corresponding to $\Omega_{f_1g}, \Omega_{f_2g}, \Omega_{f_3g}, \Omega_{f_4g}, \Omega_{f_5g} = \Omega_{f_6g}$. Projections along Ω_3 axis shows two peaks for $|\mathcal{S}_i(\Omega_3, \Omega_2, 0)|$ (Fig. 6(b,bleft column)) resonant with frequencies $\Omega_{e_1g}, \Omega_{e_2g} \approx \Omega_{e_3g}$. For $|\mathcal{S}_{ii}(\Omega_3, \Omega_2, 0)|$ (Fig. 6(b,bmiddle column)) we would ideally expect eighteen peaks corresponding to $\Omega_{f_1e_3}, \Omega_{f_1e_2}, \Omega_{f_3e_4}, \Omega_{f_4e_2}, \Omega_{f_2e_3}, \Omega_{f_2e_2}, \Omega_{f_1e_1}, \Omega_{f_3e_3}, \Omega_{f_3e_2} = \Omega_{f_4e_1} = \Omega_{f_6e_3}, \Omega_{f_6e_2}, \Omega_{f_5e_3}, \Omega_{f_2e_1}, \Omega_{f_5e_2}, \Omega_{f_3e_1}, \Omega_{f_6e_1}, \Omega_{f_5e_1}$ in energetically increasing order. However, only twelve peaks are observed due to overlapping caused by anharmonicities and coupling strength. Similar to Amide-I vibrations of NMA in cavity, we observe fewer peaks in $|\mathcal{S}(\Omega_3, \Omega_2, 0)|$ (Fig. 6(b, right column)) than that of $|\mathcal{S}_{ii}(\Omega_3, \Omega_2, 0)|$ due to destructive

interferences between $|\mathcal{S}_{ii}(\Omega_3, \Omega_2, 0)|$ and $|\mathcal{S}_i(\Omega_3, \Omega_2, 0)|$.

Strong coupling regime $\widetilde{g} = 50 cm^{-1}$ *(Fig. 6(c)):* Increasing coupling resolves the six bipolariton resonances along Ω_2 for all contributions to the DQC signal (Fig. 6(c)). Along Ω_3 axis, however, only $|\mathcal{S}_i(\Omega_3, \Omega_2, 0)|$ is more resolved with three peaks corresponding to $\Omega_{e_1 g}$, $\Omega_{e_2 g}$ and $\Omega_{e_3 g}$ with splitting $\sim \widetilde{g}_i$. Despite better peak resolution due to coupling strength dependent peak separations, resonances due to overlapping peaks cannot be fully resolved. The total signal (Fig. 6(right column)) only has 10 distinct peaks as a result of destructive interference of energies of $\Omega_{e_2 g}$ and $\Omega_{e_3 g}$ with some of the resonances from $|\mathcal{S}_{ii}(\Omega_3, \Omega_2, 0)|$.

Increasing coupling strengths provides us well resolved molecular vibrational bipolariton manifold structure (along Ω_2 axis), however, it may not provide well resolved DQC signals along Ω_3 axis requiring a careful tuning of $\widetilde{g}_i$.

V.   CONCLUSIONS

The Multidimensional DQC signals shown in Figs. 2 - 6 demonstrate how the ground state vibrational excitation manifolds are modified upon coupling to the cavity modes. The anharmonicities in the case of Amide-I of NMA coupled to cavity (for non-zero detuning $\delta \neq 0$) are modified with cavity coupling strength, $\Delta_{ij} \to \widetilde{V}_{ij} = 16\Delta_{11}|\widetilde{g}_1^4/(\delta^2 - 16\widetilde{g}_1^2)^2|$ and this can be observed in the peak splitting. For zero detuning, the anharmonicitiy is independent of coupling strength, i.e., $\lim_{\delta \to 0} \widetilde{V}_{ij} = \Delta_{11}/32$. However, in the case of Amide-I+II of NMA coupled to the infrared cavity anharmonicities in polariton basis varying nontrivially by, $\widetilde{V}_{ij} = 1/2\Delta_{ij}|X_i|^2|X_j|^2$ where, $X_{i/j}$ depend on higher order of coupling strengths. This causes several peaks to overlap beyond certain cavity coupling and this is why not all expected peaks for Ω_{fe} can be spectrally resolved in Fig. 6. However, we can use cavity coupling dependent anharmonicities for modifications of ground vibrational structures to mimic weakly interacting molecular vibrational multi-modes.

Controlling and manipulating lifetime of single molecular vibrations by tuning the coupling strengths and time delays between ultrafast pulses (say, t_1) can reveal new energy transfer mechanisms. Varying cavity polarization ($\boldsymbol{\mu}_k \cdot \boldsymbol{e}_c$) and incident angle ($\theta$) in Eq. 1 using collinear experiments[27] could provide information regarding spatial confinements of several vibrational excitations and possibilities of molecular vibrational condensates like usual electronic polariton condensates in organic[39–41] and inorganic[39,42,43] microcavities, if

11

effective dense vibrational polaritons are obtained, which may be possible in larger macro-molecules like J-aggregates. Time-varying cavity coupling strengths can be used to study dynamics of efficient cooling of molecular vibrational states for $n-polariton$ manifolds using higher dimensional spectroscopic techniques.

This work can be extended to control collective molecular vibrational excitations, which may be a useful tool in molecular cooling[44] allowing to perform ultracold experiments even at room-temperature. Furthermore, by varying the time delays one could be able to modify molecular vibrations via cavity and catch them in action in real time. We show that, by varying the cavity coupling strength $(\widetilde{g})$, it is possible to retrieve spectrally well-resolved molecular vibrational polariton(bipolariton) resonances which are otherwise difficult to re-solve (see Fig. 2 - 6 for example). Similar results with respect of the anharmonicities and peak redistributions due to cavity coupling can be achieved using other 2DIR techniques, e.g. $\boldsymbol{k_s} = -\boldsymbol{k}_1 + \boldsymbol{k}_2 + \boldsymbol{k}_3$ or $\boldsymbol{k_s} = \boldsymbol{k}_1 - \boldsymbol{k}_2 + \boldsymbol{k}_3$, however, the full power of DQC mea-surements presented here for single molecule in optical cavity can be seen more easily for macromolecules. For such larger systems, a different and much faster numerical algorithms utilizing techniques similar to Nonlinear Exciton Equations (NEE)[32] will be useful. Studying the dynamics of modified electronic ground states by applying methods developed in Ref.[26] can also be done. In addition, incorporating electronic states can similarly be achieved to modify vibrational excitations of electronically excited states.

ACKNOWLEDGMENTS

REFERENCES

[1] P. R. Berman, *Cavity quantum electrodynamics* (Academic Press, Inc., Boston, MA (United States), 1994).

[2]S. Haroche and J. M. Raimond, *Exploring the quantum* (Oxford Univ. Press, 2006).

[3]D. M. Coles, Y. Yang, Y. Wang, R. T. Grant, R. A. Taylor, S. K. Saikin, A. Aspuru-Guzik, D. G. Lidzey, J. K.-H. Tang, and J. M. Smith, Nature communications **5** (2014).

[4]D. M. Coles, N. Somaschi, P. Michetti, C. Clark, P. G. Lagoudakis, P. G. Savvidis, and D. G. Lidzey, Nature materials **13**, 712 (2014).

[5]F. Herrera, B. Peropadre, L. A. Pachon, S. K. Saikin, and A. Aspuru-Guzik, The Journal of Physical Chemistry Letters **5**, 3708 (2014).

[6]A. Shalabney, J. George, J. Hutchison, G. Pupillo, C. Genet, and T. W. Ebbesen, Nature communications **6** (2015).

[7]J. del Pino, J. Feist, and F. J. Garcia-Vidal, New Journal of Physics **17**, 053040 (2015).

[8]A. Shalabney, J. George, H. Hiura, J. A. Hutchison, C. Genet, P. Hellwig, and T. W. Ebbesen, Angewandte Chemie International Edition **54**, 7971 (2015).

[9]B. Simpkins, K. P. Fears, W. J. Dressick, B. T. Spann, A. D. Dunkelberger, and J. C. Owrutsky, ACS Photonics (2015).

[10]T. Autry, G. Nardin, D. Bajoni, A. Lemaître, S. Bouchoule, J. Bloch, and S. Cundiff, in *CLEO: QELS_Fundamental Science* (Optical Society of America, 2015), pp. FW4B–7.

[11]Y. Sun, Y. Yoon, M. Steger, G. Liu, L. N. Pfeiffer, K. West, D. W. Snoke, and K. A. Nelson, arXiv preprint arXiv:1508.06698 (2015).

[12]B. L. Wilmer, F. Passmann, M. Gehl, G. Khitrova, and A. D. Bristow, Physical Review B **91**, 201304 (2015).

[13]V. Savona, L. Andreani, P. Schwendimann, and A. Quattropani, Solid State Communications **93**, 733 (1995).

[14]J. Feist and F. J. Garcia-Vidal, Physical Review Letters **114**, 196402 (2015).

[15]S. Faez, P. Türschmann, H. R. Haakh, S. Götzinger, and V. Sandoghdar, Physical review letters **113**, 213601 (2014).

[16]A. Alù, M. G. Silveirinha, A. Salandrino, and N. Engheta, Physical Review B **75**, 155410 (2007).

[17]R. Fleury and A. Alù, Physical Review B **87**, 201101 (2013).

[18]H. Kelkar, D. Wang, B. Hoffmann, S. Christiansen, S. Götzinger, and V. Sandoghdar, in *European Quantum Electronics Conference* (Optical Society of America, 2015), p. EG_6_1.

[19]A. Benz, S. Campione, J. F. Klem, M. B. Sinclair, and I. Brener, Nano letters **15**, 1959 (2015).

[20]Z. Lai, N. K. Preketes, S. Mukamel, and J. Wang, The Journal of Physical Chemistry B **117**, 4661 (2013).

[21]D. Abramavicius, D. V. Voronine, and S. Mukamel, Proceedings of the National Academy of Sciences **105**, 8525 (2008).

[22]R. Venkatramani and S. Mukamel, The Journal of chemical physics **117**, 11089 (2002).

[23]A. Piryatinski, V. Chernyak, and S. Mukamel, Chemical Physics **266**, 311 (2001).

[24]C. Greve, N. K. Preketes, H. Fidder, R. Costard, B. Koeppe, I. A. Heisler, S. Mukamel, F. Temps, E. T. Nibbering, and T. Elsaesser, The Journal of Physical Chemistry A **117**, 594 (2013).

[25]J. A. Cwik, P. Kirton, S. De Liberato, and J. Keeling, arXiv preprint arXiv:1506.08974 (2015).

[26]S. Mukamel, *Principles of nonlinear optical spectroscopy*, 6 (Oxford University Press, 1999).

[27]G. Nardin, Semiconductor Science and Technology **31**, 023001 (2015).

[28]N. Takemura, S. Trebaol, M. Anderson, V. Kohnle, Y. Léger, D. Oberli, M. T. Portella-Oberli, and B. Deveaud, Physical Review B **92**, 125415 (2015).

[29]H. Oka and H. Ishihara, Physical Review B **78**, 195314 (2008).

[30]H. Oka and H. Ishihara, Physical review letters **100**, 170505 (2008).

[31]V. Chernyak, W. M. Zhang, and S. Mukamel, The Journal of chemical physics **109**, 9587 (1998).

[32]D. Abramavicius, B. Palmieri, D. V. Voronine, F. Sanda, and S. Mukamel, Chemical reviews **109**, 2350 (2009).

[33]O. Roslyak, G. Gumbs, and S. Mukamel, Nano letters **10**, 4253 (2010).

[34]See supplemental material at [URL will be inserted by AIP] for total Hamiltonian of system in polariton basis and respective singly and doubly excited manifold (Eq Figures S1-S10 show dispersive and absorptive parts of the DQC signals shown in maintext. Figure S11- respective peak splittings.

[35]T. Hayashi and S. Mukamel, Journal of molecular liquids **141**, 149 (2008).

[36]I. V. Rubtsov, J. Wang, and R. M. Hochstrasser, The Journal of Physical Chemistry A **107**, 3384 (2003).

[37]A. Barth, Biochimica et Biophysica Acta (BBA)-Bioenergetics **1767**, 1073 (2007).

[38]L. P. DeFlores, Z. Ganim, S. F. Ackley, H. S. Chung, and A. Tokmakoff, The Journal of

Physical Chemistry B **110**, 18973 (2006).

[39] H. Deng, H. Haug, and Y. Yamamoto, Reviews of modern physics **82**, 1489 (2010).

[40] E.R. Bittner, S. Zaster, and C. Silva, Phys. Chem. Chem. Phys, **14**, 3226-3233 (2012).

[41] S. Zaster, and E. R. Bittner, International Journal of Modern Physics B **29**, 1550157 (2015).

[42] J. Kasprzak, M. Richard, S. Kundermann, A. Baas, P. Jeambrun, J. Keeling, F. Marchetti, M. Szymańska, R. Andre, J. Staehli, et al., Nature **443**, 409 (2006).

[43] J. D. Plumhof, T. Stöferle, L. Mai, U. Scherf, and R. F. Mahrt, Nature materials **13**, 247 (2014).

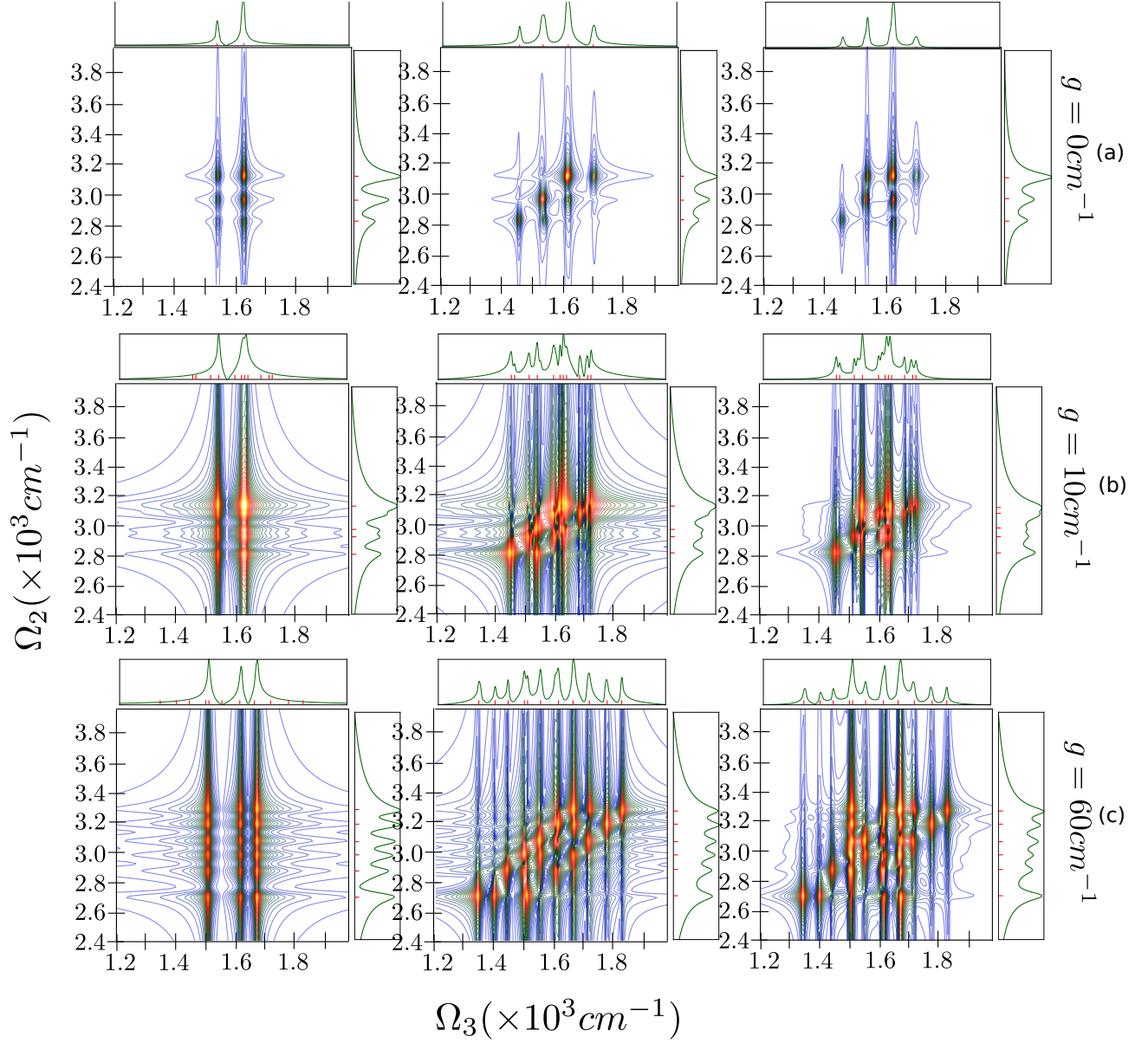[44] M. Kowalewski, G. Morigi, P. W. Pinkse, and R. de Vivie-Riedle, Physical Review A **84**, 033408 (2011).

FIG. 6: DQC signals for Amide-I+II vibrations in NMA using Eq. 3 and ladder diagrams

(Fig. 1e): *Columns* : (left-)$|\mathcal{S}_i(\Omega_3, \Omega_2, 0)|$ with resonance at Ω_{e_1g}, Ω_{e_2g} and Ω_{e_3g} ;

(middle-)$|\mathcal{S}_{ii}(\Omega_3, \Omega_2, 0)|$ with resonance at $\Omega_{f_1e_3} \approx \Omega_{f_1e_2}$, $\Omega_{f_3e_4} \approx \Omega_{f_4e_2}$, $\Omega_{f_2e_3} \approx \Omega_{f_2e_2}$, $\Omega_{f_1e_1}$,

$\Omega_{f_3e_3} \approx \Omega_{f_3e_2} = \Omega_{f_4e_1} = \Omega_{f_6e_3}$, $\Omega_{f_6e_2}$, $\Omega_{f_5e_3}$, $\Omega_{f_2e_1}$, $\Omega_{f_5e_2}$, $\Omega_{f_3e_1}$, $\Omega_{f_6e_1}$, $\Omega_{f_5e_1}$ and

(right-)$|\mathcal{S}(\Omega_3, \Omega_2, 0)|$ with respective resonances and cavity couplings (*rows*) (a)$0cm^{-1}$,

(b)$10cm^{-1}$, and (c) $60cm^{-1}$ along Ω_3, while peaks at Ω_{f_1g},Ω_{f_2g},Ω_{f_3g},Ω_{f_4g},Ω_{f_5g} and Ω_{f_6g}

along Ω_2. The linear projections along each axis is shown in green. For simplicity, cavity

field vector $\boldsymbol{e}_c$ is assumed to be mostly parallel to molecular vibrational transition dipole

μ_m. Amide-I vibrations (ω_1) is resonant to cavity cutoff frequency $\omega_0 = 1625cm^{-1}$ and

$\omega_2 = 1540cm^{-1}$. The anharmonicities are assumed $\Delta_{11} = 15cm^{-1}$ and $\Delta_{22} = 11cm^{-1}$

(Table I)

16